Controlling Optical Properties and Function of BODIPY by Using Asymmetric Substitution Effects

Jorge Bañuelos-Prieto,*[a] Antonia R. Agarrabeitia,[b] Inmaculada Garcia-Moreno,[c] Iñigo Lopez-Arbeloa,[a] Angel Costela,[c] Lourdes Infantes,[c] M. Eugenia Perez-Ojeda,[c] Marta Palacios-Cuesta,[b] and María J. Ortiz*[b]

Abstract: Asymmetrically substituted BODIPY analogues of the dye PM567 have been synthesised from 2-acylpyrroles and pyrroles that bear indene, fluorene or difluorene units. The type of linkage between the fluorene and the BODIPY core plays an important role in the photophysics of the BODIPY chromophore. Indeed, an aliphatic bridge gives rise to an energy-transfer process between the chromophores, whereas a vinyl spacer allows an electronic interaction between them, leading to a large red shift of the spectral bands. The laser action of the new dyes has been analysed under transversal pumping at 10 Hz repetition rate, in both liquid phase and incorporated into solid polymeric matrices. Lasing efficiencies of up to 40% were reached with high photostabilities with the laser output remaining at the initial level after 1×10^5 pump pulses in the same position of the sample. The laser action of the new dyes outperforms the laser behaviour of commercial dyes that emit in the same spectral region. The replacement of fluorene by indene quenches the fluorescence and laser emission, but allows the development of an iron cation fluorescent sensor.

Keywords: BODIPY · fluorescence · laser chemistry · pyrroles · sensors

Introduction

Fluorescent dyes based on 4,4-difluoro-4-bora-3a,4a-diaza-*s*-indacene derivatives, known as BODIPYs, are widely used as the active media for tuneable lasers, as they have a low intersystem crossing rate, hence low triplet–triplet absorp-tion probability over the lasing spectral region, and are very photostable. They present absorption and emission bands in the green-yellow and red part of the visible electromagnetic spectrum and a fluorescence quantum yield, in some cases, near unity.[1] Their laser action is even better than that of rhodamine dyes,[2] considered as the benchmark in laser per-formance.

Although the lasing action of the BODIPY dyes has been the focus of much research,[1] more effort is needed to en-hance their photostability, especially for commercial applica-tions. It has been demonstrated that the modification of the molecular structure of the chromophore system with ade-quate substituents can give rise to more photostable laser dyes with better photophysical and optical properties. Thus, the synthesis of analogues of the most extensively used laser dye, PM567 (Scheme 1), has been undertaken by incorporat-ing several substituents on the pyrromethene moiety.[3]

To our knowledge, the studies on BODIPY dyes with flu-orene units have been limited to structurally rigid BODIPY dyes with spirofluorene moieties,[4] polymeric and copoly-meric BODIPY dyes[5] and systems containing alkynylfluor-ene units linked to the different positions.[6] In particular systems with the indene chromophore have not been report-ed.

[a] Dr. J. Bañuelos-Prieto, Dr. I. Lopez-Arbeloa
Departamento de Quimica Fisica
UPV-EHU, Apartado 644
48080 Bilbao (Spain)
Fax: (+34) 946013500
E-mail: jorge.banuelos@ehu.es

[b] Prof. A. R. Agarrabeitia, M. Palacios-Cuesta, Prof. M. J. Ortiz
Departamento de Quimica Organica I
Facultad de Ciencias Quimicas
Universidad Complutense
28040 Madrid (Spain)
Fax: (+34) 913944103
E-mail: mjortiz@quim.ucm.es

[c] Dr. I. Garcia-Moreno, Dr. A. Costela, Dr. L. Infantes,
M. E. Perez-Ojeda
Instituto de Quimica-Fisica "Rocasolano" (IQFR)
CSIC, Serrano 119
28006 Madrid (Spain)

Supporting information for this article is available on the WWW under http://dx.doi.org/10.1002/chem.201002095.
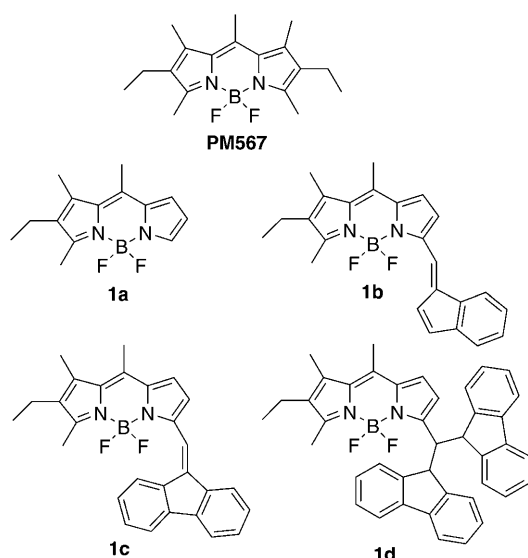
Scheme 1. Molecular structures of commercial dye PM567 and their analogues **1a–d** synthesised in this work.

Introduction of these substituents at the appropriate position of the indacene core could be carried out by reaction over the BODIPY previously synthesised or by modification of the pyrrole starting material in the BODIPY synthesis.[3c,f] In this last method, asymmetric BODIPY dyes are usually obtained by condensation of a carbonyl-containing pyrrole with a pyrrole molecule that is not substituted at the 2-position. Linked fluorene–pyrrole and indene–pyrrole ensembles through C=C bonds are unknown. At the same time, such compounds are especially promising as starting materials for the synthesis of novel BODIPY fluorophores, owing to the extension of the overall conjugation.

The work carried out covers these aspects, and describes the synthesis of new asymmetric BODIPY dyes, PM567 analogues **1a–d**, for which fluorene and indene units have been incorporated into one of the pyrrole rings (Scheme 1). The alkyl substituted dye, **1a**, was synthesised as reference to assess the effect of incorporating fluorene and indene moieties at its 5-position.
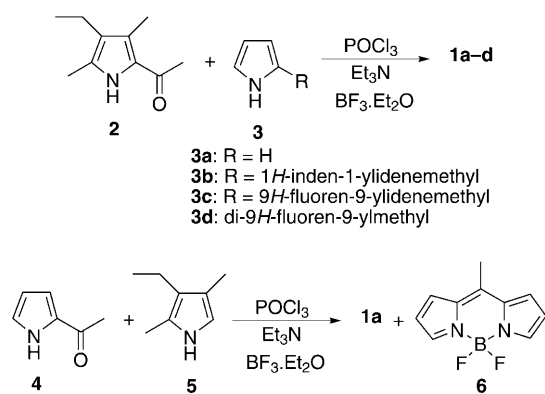
Initially, we considered if the synthetic strategy previously described by our research group, to achieve systems 1,4-unsaturated with 1-indenylidene and 9-fluorenylidene units,[7] could be employed for the synthesis of new pyrrole structure with an α-position substituted for above chromophores. Surprisingly, we obtained the desired pyrroles, but with some unexpected results, and from these systems we carried out the corresponding asymmetric BODIPY dyes.

In addition, we report here the evaluation of the photophysical properties and laser behaviour of the new dyes both in solution and solid media. The BODIPY bearing two fluorene groups connected via a methylene group is found to have a very high fluorescence capacity (close to the unit, regardless of the solvent), lasing efficiency and photostability, improving the characteristics of the commercially available PM567. However, if the linkage between BODIPY and

fluorene is performed by a vinyl group the resonant interaction between both electronic clouds leads to a red emitting dye, but with lower fluorescence and lasing efficiency. On the other hand, a BODIPY bearing an indene unit, also linked by a vinyl group, shows very low red fluorescent emission, but is sensitive to the presence of iron cations in the surrounding environment. Thus, such system could be used as a fluorescent sensor.

Results and Discussion

Synthesis of the dyes: The new asymmetric dyes **1a–d** were obtained by condensation of 2-acetyl-4-ethyl-3,5-dimethyl-pyrrole[8] (**2**) with a pyrrole molecule (**3**) conveniently substituted at the 2-position, following conditions previously described[9] (Scheme 2).

3a: R = H
3b: R = 1H-inden-1-ylidenemethyl
3c: R = 9H-fluoren-9-ylidenemethyl
3d: di-9H-fluoren-9-ylmethyl

Scheme 2. Synthetic scheme for compounds **1a–d**.

The reaction of **2** and pyrrole with phosphorus oxychloride followed by treatment with boron trifluoride etherate in the presence of triethylamine yielded the BODIPY dye **1a** (26%) and another dye that was identified as BODIPY PM567 (4%). An alternative route from 2-acetylpyrrole (**4**) and 3-ethyl-2,4-dimethylpyrrole (**5**) yielded **1a** (46%) and traces of 8-methyl-4,4-difluoro-4-bora-3a,4a-diaza-s-indacene (**6**)[11] (Scheme 2). This route gave highest yield of the desired dye.

The presence of secondary products (PM567 and **6**) involves the reaction of **2** or **4** with their respective deacetylated products, however, there is not examples in the literature of deacetylation of pyrroles, but the decarboxylation reaction of 2- or 3-pyrrole carboxylic acids is very common.[10] A possible explanation involves the haloform reaction to give the corresponding carboxylic acid, which loses carbon dioxide, although, in this reaction a trichloro compound is required and its formation is speculative. An alternative mechanism for the formation of compounds prepared from compounds **2** and **3a**, or **4** and **5**, is included in Scheme 3. This mechanism is based on the facts that the formation of the sigma-complex in course of an electrophilic (het)aromatic substitution is a reversible process. Thus, the reaction of **2** or
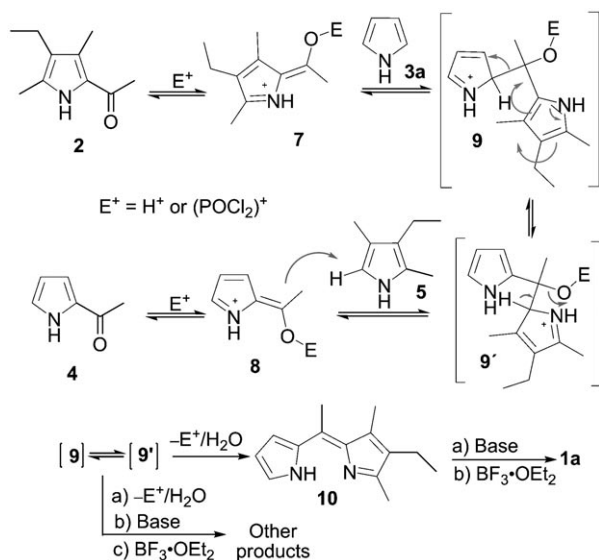
Scheme 3. Mechanism proposed for the formation of **1a** and the secondary products.

4 with an electrophile gives **7** and **8**, respectively, that by reaction with the corresponding pyrroles afforded the intermediates **9** and **9'**, which yield the dipyrromethene **10** the precursor of **1a**. These intermediates are essential in the proposed mechanism, and other secondary products observed in the reaction could be justified from them.

BODIPY **1b** was formed by reaction of **2** and **3b**, which was synthesised from *N*-protected pyrrole 2-carbaldehyde (**11**) and indene, as shown in Scheme 4, following the condi-
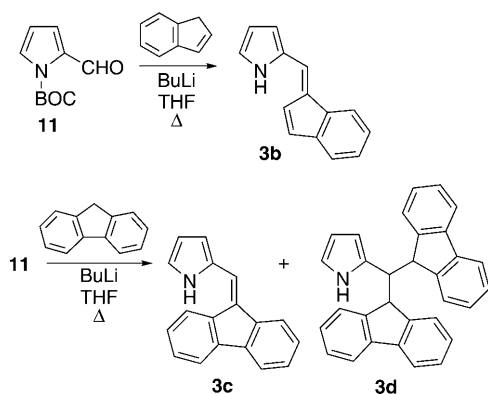
Scheme 4. Synthetic scheme for pyrroles **3b–d**.

tions previously described in our laboratory.[7] However, when compound **11** was reacted with fluorene in the same conditions, **3c** was obtained along with a new compound that was identified as **3d** (Scheme 4).

Possible mechanistic pathway for formation of **3d** involves the intermediary anion **12**, which attacks the C=C bond present in the *N*-protected pyrrole **13** (Scheme 5). This attack could be justified by the high stability of anion **14**, in
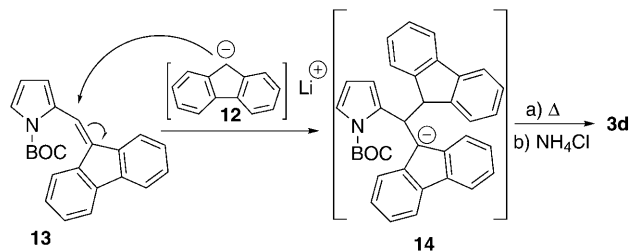
Scheme 5. Possible mechanistic pathway for formation of **3d**.

which the negative charge is delocalised by conjugation with two benzene rings.

To remove the formation of pyrrole **3d**, we carried out the synthesis of **3c** in Suzuki cross-coupling reaction between *N*-protected pyrrole 2-boronic acid (**15**) and 9-bromomethylene-9*H*-fluorene (**16**),[12] as shown in Scheme 6. In these conditions, only **3c** was obtained, although also in low yield.
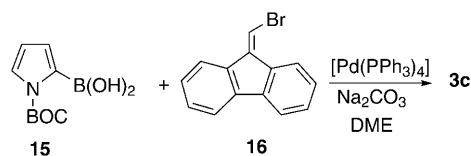
Scheme 6. Alternative route for the formation of **3c**.

Pyrroles **3c** and **3d** were later employed in the synthesis of **1c** and **1d**, respectively, according to the reactions indicated in Scheme 2. Traces of PM567 were observed in both cases. The structures of BODIPY dyes **1b–d** were confirmed by single-crystal X-ray diffraction (Figure 1 and the Supporting Information).

Photophysical properties: The asymmetrically alkyl-substituted **1a** dye shows some of the typical photophysical fea-

Figure 1. ORTEP representation of the molecular structure of BODIPY **1d**.
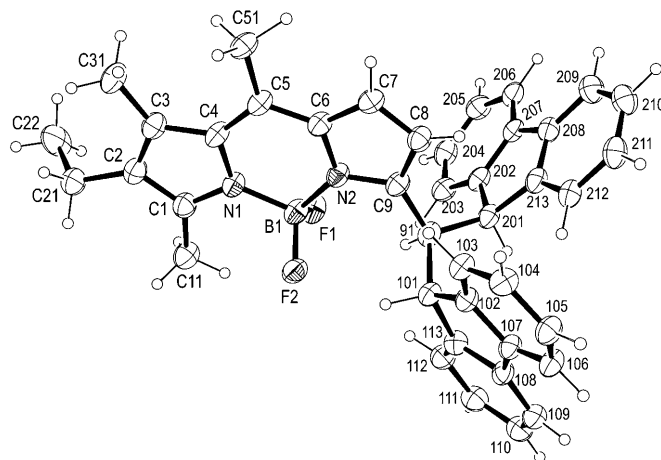
Table 1. Photophysical properties, under visible excitation, of **1a**, **1c** and **1d** in apolar, polar and polar/protic solvents.

Solvent	λ_{abs}[a]	ε_{max}[b]	λ_{flu}[a]	ϕ[c]	τ[d]	k_{fl}[e]	k_{nr}[e]	$\Delta\nu_{St}$[f]
Dye 1a								
F3-ethanol	492.0	1.9	511.0	0.75	6.17	1.21	0.40	760
methanol	495.5	2.5	512.5	0.76	5.78	1.31	0.41	660
ethanol	497.0	2.5	513.5	0.84	5.73	1.46	0.28	630
acetone	495.0	2.2	512.5	0.79	5.66	1.39	0.37	690
ethyl acetate	496.0	2.5	512.5	0.84	5.57	1.50	0.28	650
c-hexane	504.0	3.3	515.0	0.96	5.46	1.75	0.07	735
Dye 1c								
F3-ethanol	566.5	4.1	600.5	0.33	2.28	1.44	2.93	995
methanol	575.4	5.0	603.5	0.48	3.20	1.50	1.62	805
ethanol	579.0	5.1	605.5	0.58	3.67	1.58	1.14	765
acetone	574.0	4.3	603.5	0.47	2.91	1.61	1.82	855
ethyl acetate	578.0	5.0	605.5	0.65	3.78	1.72	0.92	790
c-hexane	589.0	5.6	611.5	0.73	4.07	1.79	0.66	615
Dye 1d								
F3-ethanol	510.5	2.1	523.5	1.0	6.26	1.59	0	490
methanol	512.5	3.9	525.0	0.99	5.76	1.72	0.02	455
ethanol	514.0	4.2	526.0	0.93	5.59	1.66	0.12	440
acetone	511.5	3.9	525.5	0.99	5.61	1.76	0.02	480
ethyl acetate	513.5	4.0	525.0	0.94	5.47	1.72	0.11	450
c-hexane	521.0	5.0	529.5	0.97	5.20	1.86	0.05	320

[a] Absorption (λ_{abs}) and fluorescence (λ_{flu}) wavelength (± 0.5 nm). [b] Molar absorption (ε_{max}, $10^4 \, M^{-1} cm^{-1}$). [c] Fluorescence quantum yield (ϕ, ± 0.05). [d] Fluorescence lifetime (τ, ± 0.05 ns). [e] Radiative (k_{fl}) and non-radiative (k_{nr}) rate constants ($10^8 \, s^{-1}$). [f] Stokes shift ($\Delta\nu_{St}$, cm^{-1}).
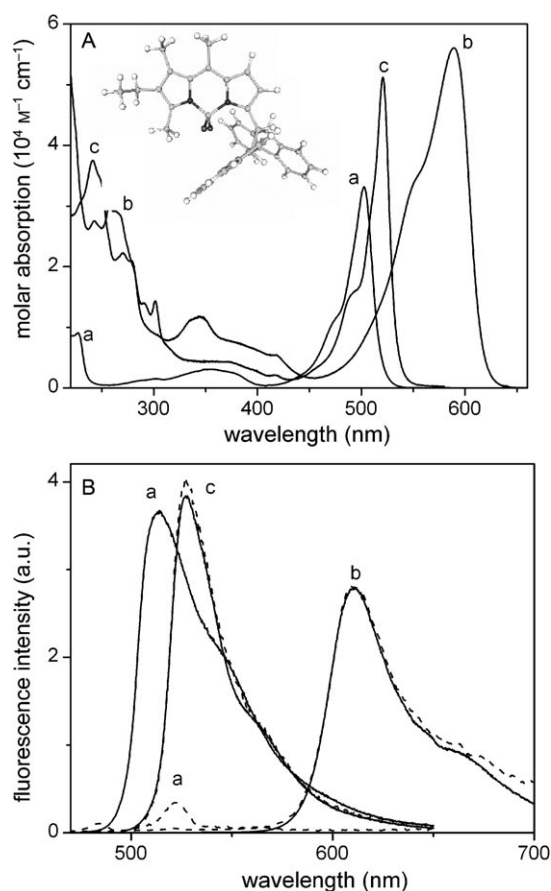

Figure 2. A) UV/Vis absorption spectra of **1a** (a), **1c** (b) and **1d** (c) in diluted solutions of c-hexane. B) Fluorescence spectra under visible excitation (solid line) and under UV excitation (dashed line). Inset A: optimised ground state geometry of **1d**.

tures of the BODIPY chromophore,[1a] as can be derived from the corresponding data summarised in Table 1. The absorption and fluorescence bands in the green-yellow part of the visible have been characterised by slight hypsochromic shifts with the solvent polarity and high fluorescence quantum yields (ϕ up to 0.95 in apolar media) and lifetime (τ around 5–6 ns). The fluorescence lifetime increases with the solvent polarity, while the fluorescence quantum yield decreases. Such evolutions are owed to a decrease of k_{fl} (correlated with the diminution of ε_{max}) and a small increase of k_{nr} in the polar media (Table 1). This behaviour, is not usual in symmetric BODIPY,[1a] and could be ascribed to the asymmetric substitution pattern affecting the transition dipole moment. Then, the alkyl substituted **1a** dye will be used as reference to discuss the effect of incorporating fluorene and indene moieties at its 5 position.

Fluorene-BODIPY derivatives: The inclusion of two fluorene units at the same position of the BODIPY core, both separated from the chromophore by a methylene group (**1d**), induces a modest bathochromic shift (around 15 nm) of the absorption and fluorescence spectral bands, with regard to the parent asymmetric **1a**, as illustrated in Figure 2. Such a shift should be a result of the donor inductive effect of the branched substituent. The evolution of the spectral bands with solvent characteristics follows the above described hypsochromic shift with the solvent polarity. The inspection of the photophysical data of this novel multichromophoric dye under visible excitation (Table 1), reveals that the inclusion of the fluorene units improves the fluorescence capacity of the BODIPY chromophore, giving rise to fluorescence quantum yield close to the unity, independent of the considered solvent.

Quantum-mechanical calculations propose a ground state geometry in which the BODIPY core and the fluorene units are disposed in different planes, nearly perpendicular between each other (inset Figure 2A). Such a conformation avoids any electronic interaction between them. Indeed, the simulation of the absorption transition predicts a bathochromic shift of around 10 nm and a similar transition probability, with respect to **1a**. Previous works pointed out that the inclusion of bulky groups with free rotation enhances the internal conversion processes, owing to the vibrational coupling, decreasing the fluorescence capacity of the dye.[13] However, in the present case, the bulkiness and disposition of the fluorene moieties, as well as their special proximity, leads to a high steric hindrance, which should hinder their rotation and hence the non-radiative pathway. Such constrained structures are characterised by improved fluorescence capacities,[3d,14] as is the present case of **1d** (Table 1).

The inspection of the UV part of the absorption spectrum of the multichromophoric BODIPY-fluorene triad reveals the presence of new bands not observed for **1a**, and hence assigned to the fluorene entity (Figure 2A), since in addition

they match perfectly with its spectrum.[15] Therefore, the whole absorption spectrum of the **1d** dye can be considered as the sum of the bands of the BODIPY core and the fluorene moiety (Figure 2A), confirming again the absence of any intermolecular interaction between both aromatic entities, at least in the ground state (Figure 2 A). On the other hand, the excitation in the UV, where just the fluorene chromophore absorbs light, leads only to the visible emission of the BODIPY dye (Figure 2B), without trace of the fluorene emission, which typically is high ($\phi \approx 0.77$).[15] Consequently, in the multichromophoric **1d** system, an efficient intramolecular excitation energy transfer (intra-EET) process takes place from the two donor fluorenes to the acceptor BODIPY core, quenching the emission of the fluorene in favour of the bright visible emission of the BODIPY. Thus, a very high "virtual" Stokes shift is achieved since the fluorescence detection region (Vis) can be monitored far away from the excitation (UV), reducing background scatter interferences.

Typically in dyads consisting of BODIPY moieties acting as donor or acceptor in the intra-EET process, two different mechanisms are responsible of the energy transfer:[16] the through-bond and the through-space mechanisms (i.e., the so-called Förster dipole–dipole coupling).[17]

The through-bond mechanism demands an orbital overlap between the donor and the acceptor (electronic coupling).[18] It has been observed with BODIPY cores acting as acceptors and bearing donor groups (i.e., polyphenyl) directly linked at *meso* position,[19] which is characterised by its high electronic density in the LUMO state. Such a mechanism has also been observed with unsaturated bridges or spacers (ethynyl) connecting the donor (anthracene) and the acceptor BODIPY core.[16c] In the present **1d** triad, the fluorene units are separated by two single bonds from the BODIPY core and the through-bond energy transfer should drastically decrease with the distance between the donor and the acceptor. Therefore, such mechanism does not seem to be the main cause of the observed efficient intra-EET process in **1d**.

The through-space process requires mainly a spectral overlap between the fluorescence band of the donor and the absorption band of the acceptor (dipole–dipole coupling) on the basis of the Förster mechanism.[20] In our case, the fluorescence band of the fluorene (placed around $\lambda = 300$ nm) hardly overlaps with the $S_0 \rightarrow S_1$ absorption band of the BODIPY core (place around $\lambda = 500$ nm), reducing the probability of the direct energy-transfer process through dipole–dipole coupling between both states. However, the fluorene emission overlaps with the more energetic absorption bands of the BODIPY chromophore ($S_0 \rightarrow S_2$ and $S_0 \rightarrow S_3$ placed around $\lambda = 350$ nm). Aside from the lower absorption probability of such transitions, it seems that such overlap is enough to allow the energy-transfer process via this mechanism. Indeed, Ziessel and co-workers have reported intra-EET processes in multichromophoric systems consisting in pyrene, terpyridine and a fluorene-derivative attached to different positions of the BODIPY core and even replac-

ing the fluorine atoms.[6a] Owing to the spectral overlap of the aromatic substituent fluorescence with the $S_0 \rightarrow S_2$ and $S_0 \rightarrow S_3$ absorption bands of the boradiazaindacene core, the proposed mechanism is a Förster type.

On the other hand, the inclusion of just one fluorene, also at the 5 position, but separated from the BODIPY core by a vinyl group (**1c**), leads to an important bathochromic shift (up to 100 nm) and a broadening of the spectral bands, mainly in absorption (Figure 2). In fact, quantum mechanical simulation of the absorption transition also predicts an important shift of the absorption band together with an increase in the oscillator strength (area under the curve), corroborating the observed widening of the absorption band. These changes are attributed to the extension of the electronic π system through the delocalised substituent. Indeed, the corresponding HOMO and LUMO contour maps presented in Figure 3 confirm that the electronic cloud of the
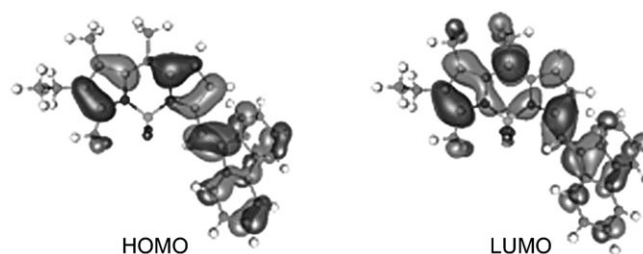

Figure 3. Electronic density of the HOMO and LUMO states of the **1c** dye.

BODIPY core is extended to the fluorene unit through the linking double bond, leading to a cyanine like delocalised π system in the whole molecule. Therefore, the type of spacer between the BODIPY and fluorene plays an important role in the photophysics of the resulting multichromophoric dye. Thus, when a saturated spacer is used (**1d**) the resonant interaction between them is avoided leading to electronically independent chromophores. However, an unsaturated bridge allows the electronic coupling between them, resulting in a delocalised new π system through the whole molecule (Figure 3).

The direct excitation of the $S_0 \rightarrow S_1$ absorption band provides a red fluorescence emission (around 600–610 nm, Figure 2B). Besides, while the absorption probability is enhanced by the extended conjugation, both the fluorescence quantum yield and the lifetime decrease with respect to the parent **1a**, due to an increase of the non-radiative deactivation rate constant (Table 1). It is known that one of the mayor drawbacks of red-emitting dyes is their lower fluorescence capacity, since the ground and excited state are energetically closer favouring: on one hand, the radiative deactivation of the emitting state (the delocalisation of the fluorene leads to higher k_{fl} values than **1a**, as correspond to the augmentation of ε_{max}, Table 1); but, on the other hand and mainly, the internal conversion probability is largely enhanced (higher k_{nr} values for **1c** than for the reference **1a**

compound), since the vibrational coupling probability between the electronic excited and ground state increases, favouring the internal conversion processes. Figure 3 shows that upon excitation the electronic density seems to shift from the fluorene (HOMO) to the BODIPY core (LUMO), reducing also the extension of the π system. The conformational changes of the unsaturated spacer connecting the BODIPY and the fluorene (i.e., rotation of this group) could participate in the augmentation of the non-radiative deactivation. As result, the emission ability is lower in the red emitting **1c**.

The photophysical properties of **1c** are clearly more sensitive to the solvent characteristics than those of the other fluorene derivative **1d** (Table 1). Thus, not only the hypsochromic shift of the spectral bands is bigger, but also the fluorescence quantum yield and lifetime clearly decrease, from c-hexane to alcohols, owing to an increase in the non-radiative deactivation rate constant. Typically, the fluorescence capacity of alkyl-BODIPYs shows a low dependency on the physicochemical properties of the solvent, being slightly higher in polar/protic environments.[1c] To get a deeper insight in the solvent effect on k_{nr}, a multilinear regression analysis has been performed, for which a physicochemical property is simultaneously correlated with different solvent properties.[21] Generally the solvent properties, which affect the photophysics of fluorophores, are those resulting from general or nonspecific interactions (polarity/polarisability) and those arising from specific interactions (acidity and basicity). These properties can be described by the Taft solvent scales (π*, α and β, respectively).[22] The corresponding regression is shown in Figure 4. The linear correlation is good ($r = 0.992$) and the fitting results indicate that the increase of k_{nr} is exclusively owed to an increase in the solvent polarity/polarisability. Recently, however, Catalan and co-workers have claimed that the term describing the solvent general interactions needs to be split into two different scales; one for the polarity (SdP) and another for polarisability (SP).[23] The solvent acidity and basicity are described by the SA and SB scales, respectively.[23] The linear fit with these four solvent scales is more accurate ($r = 0.99999$) and confirms that the solvent polarity ($c_{SdP} = 1.977$) favours the non-radiative pathway, whereas the influence of the specific interactions is negligible (Figure 4). Nevertheless, the component responsible for the evolution of k_{nr} is clearly the solvent polarisability ($c_{SP} = -6.063$). Thus, an increase of the solvent polarisability leads to a decrease of the non-radiative deactivation improving the fluorescence capacity. Indeed the evolution of k_{nr} (from 0.66×10^8 s^{-1} in c-hexane to 2.93×10^8 s^{-1} in trifluoroethanol) perfectly matches that of the solvent polarisability (SP from 0.683 to 0.543, respectively, Figure 4). In solvents of high polarisability the interactions between the π system of the dye and the solvent should be favoured, which leads to a less flexible molecular structure, but improves the fluorescence capacity of the dye.

In spite of the resonant interaction between the fluorene and the BODIPY unit, the UV absorption bands of the fluorene are still observed, and their direct excitation leads ex-
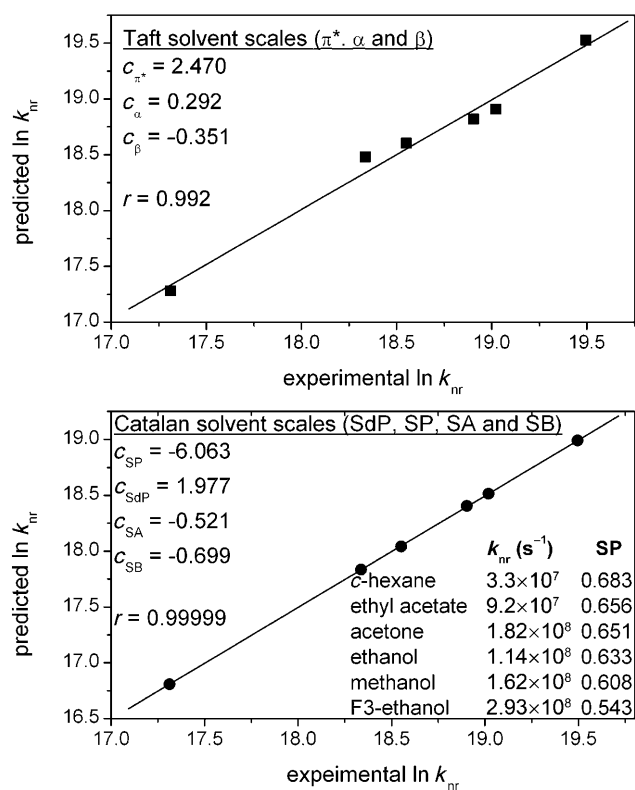

Figure 4. Multilinear regression fit of the non-radiative deactivation rate constant of **1c** on the basis of the Taft[22] solvents scales (π*, α and β describing the polarity/polarisability, acidity and basicity, respectively) and the Catalan[23] solvent scales (SdP, SP, SA and SB describing the polarity, polarisability, acidity and basicity, respectively).

clusively to the red emission of **1c**, indicating the presence of an intra-EET process that give rise to a large "virtual" Stokes shift. In this way, this bichromophoric dye converts ultraviolet light into red light. As the spacer between the donor fluorene and the acceptor BODIPY core favours the orbital overlap between them, both the through-bond and the through-space mechanism likely contribute to the intra-EET process.

Indene-BODIPY diad: The replacement of the fluorene unit by an indene moiety yields the compound **1b**. Its ground state geometry reveals that indene is disposed in a more coplanar disposition (twisting angle 20°, X-ray = 8°) with respect to the BODIPY core than fluorene (30°, X-ray = 36°). The higher planarity of the indene derivative predicted by the quantum mechanical simulation in gas phase qualitatively confirms the observed by X-ray diffraction in solid-state structures. Excitation gives rise to a more planar geometry with twisting angles of 12° for **1b** and 21° for **1c**. Such higher coplanarity in the excited state can also be derived from the HOMO and LUMO contour maps, which indicate an electronic density shift from indene to BODIPY, similar to that observed for its fluorene counterpart (Figure 3). Therefore, the indene derivative **1b** is also characterised by an extended conjugated π system, which gives rise to red-

shifted spectral bands (absorption and fluorescence band centred at $\lambda = 591$ and 596 nm, respectively in c-hexane). However, although the absorption probability remains high (ε_{max} around $6-8 \times 10^4 \, M^{-1} \, cm^{-1}$), the fluorescence quantum yield is very low, lower than 0.02. Moreover, the fluorescence decay curve is analysed by a biexponential fit consisting in a very short and dominating lifetime (19.4 ps; 95.5 %), and a minority lifetime (4.2 ns; 4.5 %), similar to typical BODIPY. Therefore, the bounding of indene to BODIPY results in a drastic increase in the non-radiative processes. Singlet oxygen generation experiments reveal that the intersystem crossing probability of **1b** remains low, as is typical of BODIPYs, owing to its quasi-aromatic π system.[24] Furthermore, viscous solvents (i.e., ethylene glycol) do not improve the photophysical behaviour of **1b**, discarding the free rotation of the indene group as the reason of the lack of fluorescence of this derivative. Thus, the non-radiative pathway should be assigned to internal conversion processes.

Previously, it has been reported that fluorene itself is characterised by a high fluorescence quantum yield (ϕ around 0.7),[15] and its linkage to BODIPY leads to a highly fluorescent laser dye. Indene, however, is characterised by a poor fluorescence signal (ϕ around 0.005), because its excited states are described as biradicals.[25] Moreover, high level computational studies have simulated the potential energy curve of the excited state looking for conical intersections between S_1 and S_0 to account for the non-radiative processes of indene.[26] They found that the main mechanism involved is a fast and efficient internal conversion process. Therefore, the linkage of indene to BODIPY, via a vinyl group, results in a negative effect on the fluorescence capacity of the BODIPY chromophore, owing, probably, to the internal conversion of the indene group.

Although **1b** is not useful for lasing applications, it is widely known that cyclopentadienyl and its derivatives (indene) form stable complexes with iron cations, for example ferrocenes.[27] Moreover, there are several fluorescent sensors based on BODIPY, commonly bearing crown ethers, to detect the presence of cations, depending of its size.[28] The binding of the cation deactivates the quenching of the crown ether (i.e., photoinduced electron transfer) and restores the fluorescence emission of the BODIPY (switches on/off). Thus, we decided to explore this possibility and make a titration experiment adding Fe^{3+} to a solution of **1b**. Although the absorption spectra remains nearly unaltered, a progressive increase of the fluorescence intensity with Fe^{3+} content was observed, as is illustrated in Figure 5. Commonly the presence of a paramagnetic ion, like Fe^{3+}, enhances the spin-orbit coupling, and hence the intersystem crossing probability, quenching the fluorescence emission. However, in the present case the interaction between iron cation and indene seems to decrease its negative effect on the BODIPY emission. Indeed, for low amounts of Fe^{3+} the fluorescence intensity is very sensitive to the presence of this cation (Figure 5). For higher concentrations ($> 4 \times 10^{-3} \, M$) the fluorescence intensity enhancement is not so prominent, but a linear relationship is obtained, which could

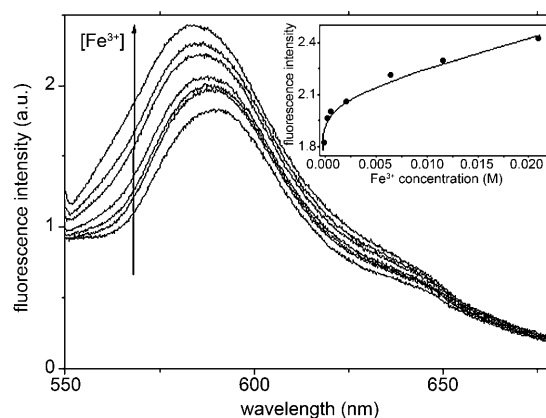Figure 5. Fluorescence spectra of **1b** for different amounts of Fe^{3+}. Inset: Evolution of the fluorescence intensity with Fe^{3+} concentration.

be used as a calibration curve to determine the concentration of the iron cation in the solution (Figure 5). Thus, **1b** should behave as a fluorescence sensor of Fe^{3+} allowing monitor quantitatively its concentration in the surrounding environment of the indene-BODIPY derivative.

Lasing properties

Liquid phase: Initially, the laser derivatives were pumped at the usual wavelength of $\lambda = 532$ nm. In our experimental setup an optical density of the dye samples of approximately 20 determines that the incoming pump radiation penetrates the sample (i.e., is absorbed) a depth similar to that to the thickness of the pump stripe at the input face of the cell onto which the pumping radiation is focused (about 0.3 mm). This gives rise to an emitted beam with near circular-cross-section and enhances the laser efficiency (ratio between the energy of the dye laser output and the energy of the pump laser incident on the sample surface).

The low absorption of the new dyes at $\lambda = 532$ nm demanded the preparation of highly concentrated solutions to reach the required optical density. This resulted in solubility problems, as well as an aggregation of dye molecules, which prevented the laser action or, in the best cases, decreased the lasing efficiency to a mere 0.6 %. Thus, we proceeded to analyse the laser behaviour of the new dyes pumped transversely with radiation with wavelength near to the absorption maximum of the dyes.

Under these experimental conditions, broad-line-width laser emission with pump threshold energy of approximately 0.8 mJ, beam divergence of approximately 5 mrad and pulse duration of approximately 8 ns FWHM was obtained from the new dyes when placed in a simple plane-plane non-tuneable resonator. The dependence of the laser action of the new BODIPY derivatives on the corresponding dye concentration was analysed in ethyl acetate varying the optical densities while keeping constant all the other experimental parameters. The lasing behaviour of the new dyes, **1a**, **c** and **d** (Figure 6), shows good correlation with their photophysical properties in dilute solutions. 1) the asymmetric substitution
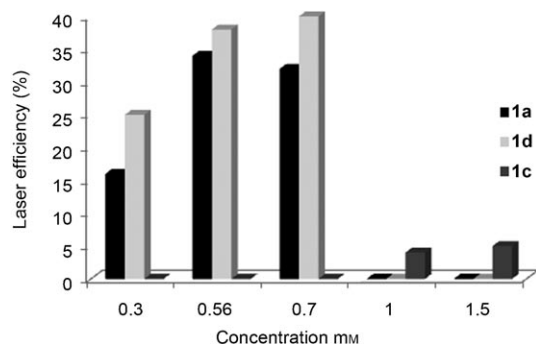
Figure 6. Lasing efficiencies of the new dyes **1a** (back bars), **1c** (dark grey bars) and **1d** (grey bars) in ethyl acetate as a function of the dye concentration.

in the BODIPY core (dye **1a**) induces highly efficient (up to 34%) laser emission peaked at approximately 530 nm, which correlates with a high fluorescence quantum yield; 2) the presence of one fluorene group red-shifts the laser emission up to $\lambda = 610$ nm and reduces drastically the conversion efficiency; 3) the presence of two fluorene groups at 3-position of BODIPY core allows to recover a high efficient (up to 40%) laser action centred at approximately 540 nm.

The actual effect of the solvent on the dye laser action was analysed in solutions of polar nonprotic and polar protic solvents at the dye concentrations that optimised the corresponding laser efficiency of each derivative. The low solubility of these new dyes in apolar solvent prevented us from producing too highly concentrated solutions that were required for some of the laser experiments under the pumping conditions selected in the present work. Once again, photophysical and laser properties are correlated: the higher the fluorescence quantum yield is, the higher the lasing efficiency becomes. Thus, the laser action of **1a** dye in acetone exhibits an efficiency of 28%, lower than those registered in ethanol (37%) and ethyl acetate (34%). The substitution of ethyl acetate by acetone as **1d** solvent increases the laser efficiency, which reaches a value of 43%.

To analyse the lasing photostability of these dyes, some studies were carried out under experimental conditions identical to those selected to irradiate the fluorophores embedded in solid polymeric matrices, which will allow later comparison of their stability in liquid and solid phases under laser irradiation. The new dyes were dissolved in ethyl acetate and their concentrations were adjusted so that the laser action was optimum in all cases. Because the irradiated volume of the solid samples in our experimental conditions was estimated to be 10 μL, capillary tubes were utilised, into which the liquid solutions were incorporated, to reproduce the geometry of the irradiated volume in the solid samples and, thus, maintaining the same laser pump conditions in both cases.

Although the optical quality of the capillary prevents laser emission from the dyes, information about their photostabilities can be obtained by monitoring the decrease in

laser-induced fluorescence intensity, under transversal excitation of the capillary, as a function of the number of pump pulses. The fluorescence emission was monitored perpendicular to the exciting beam, and its collection and analysis was carried out with the same set-up selected to characterise the laser emission from dyes incorporated into solid samples. The results obtained from the most efficient dyes, **1a** and **1d**, are plotted in Figure 7. The new dyes result to be highly
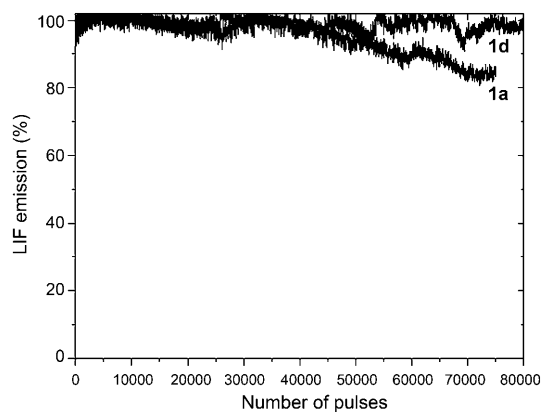

Figure 7. Normalised laser-induced fluorescence emission as a function of the number of pump pulses at 10 Hz repetition rate for **1a** and **1d** ethyl acetate solutions.

photostable since, after 80000 pump pulses at 10 Hz, the dye **1d** maintains its initial laser output without sign of degradation, while the laser emission of **1a** derivative drops by less than 10% with respect to its initial output. Once more, this laser behaviour can be related to the analysed photophysical properties: the lower the non-radiative rate constant is the higher the lasing photostability.

To put the present results in perspective, the lasing parameters of well-known dyes, such as Coumarin 540 A, which lase in the same spectral region as the studied dyes, were also measured under similar conditions. The new asymmetric dyes **1a** and **1d** exhibit laser efficiencies and photostabilities higher than the commercial Coumarin 540 A, which lases at $\lambda \approx 535$ nm with an efficiency of 25% and with a drop in the laser emission of more than 65% after 30000 pump pulses at 10 Hz.

Solid-state experiments: The experiments were carried out by using samples with the dye concentration that produced the highest lasing efficiency in ethyl acetate solution ($5-7 \times 10^{-4}$ M, depending on the dye). Methyl methacrylate (MMA) was chosen as the main monomeric component of the formulations, because this ester mimics ethyl acetate, the solvent for which the studied dyes gave rise to high lasing efficiencies. As discussed above, improvement in the lasing efficiency of **1a** dye was determined in protic polar solvents, such as ethanol. In the solid samples, the polarity of the polymeric medium can be modulated by use of appropriate copolymers. Thus, copolymers of MMA with monomers

functionalised with polar groups, such as 2-hydroxyethyl methacrylate (HEMA) were prepared in volumetric proportions ranging from 10/0 (polymethyl methacrylate (PMMA) homopolymer) to 0/10 (poly2-hydroxyethyl methacrylate (PHEMA) homopolymer).

Broad-band and efficient laser emission, with beam divergence of approximately 5 mrad and pulse duration of approximately 5 ns FWHM, was registered from the dyes incorporated as true solutions into the solid homopolymer PMMA (Table 2). No significant differences were observed

Table 2. Laser properties[a] of the new dyes incorporated in solid matrices.

Material	Eff [%]	λ_{la} [nm]	I [%]
1d/PMMA	30	542	100
1a/PMMA	20	531	94
1a (MMA/HEMA 1/1)	23	531	93
1a/PHEMA	25	532	85

[a] Eff: energy conversion efficiency, λ_{la}: peak wavelength of the laser emission; I: Intensity of the dye laser output after 100 000 pump pulses in the same position of the sample with respect to its initial intensity I_0, $I(\%) = (I/I_0) \times 100$, at 10 Hz repetition rate.

in the wavelength of the maximum laser emission of each dye between their liquid and solid solutions. The lasing efficiencies of the solid materials, in the range of 20–30%, are lower than those of the corresponding liquid solutions. In this regard, it has to be taken into account that the finishing of the surface of the solid samples relevant to the laser operation was not laser-grade, so that even higher lasing efficiencies are to be expected with laser-grade surfaces.

The lasing stabilities of the dye-doped solid matrices were studied by following the evolution of the laser output as a function of the number of pump pulses in the same position of the sample, at a 10 Hz repetition rate. Once again, both dyes exhibit a high photostability although the presence of PHEMA in the matrix degrades the lasing stability of the **1a** dye. Although the photobleaching of dyes can occur by several different mechanisms and, from a general point of view, can be considered to be quite complex, photo-oxidation, in which chemically reactive singlet oxygen is formed by sensitisation of ground-state triplet oxygen molecules by triplet state dyes,[29] is maybe the degradation mechanism most often referred to and the one with strongest relevance. The high content of HEMA in the matrix plays an important role in the photodegradation processes of dye **1a**, probably as a consequence of the higher oxygen permeability in the final material. In addition, an increase of the concentration of HEMA comonomer leads to a more plastic material, with lower elastic limit and better damage resistance.[30] However, as the internal plasticisation increases, the protecting "polymer cage" that surrounds the dye groups weakness (the polymer becomes less rigid) and, as a result, the chromophore could be easily bleached.[31]

Conclusion

In summary, new asymmetric BODIPY–indene and BODIPY–fluorene dyes have been successfully synthesised by using a conventional method. The key aspect of these syntheses is obtaining the corresponding 2-substituted pyrrole precursors, which are described for the first time in this work. These BODIPY–fluorene systems, in which both moieties are electronically decoupled, give rise to a highly fluorescent laser dye, which improves the photophysical and lasing properties of the related alkyl-BODIPYs. However, if the bridge connecting both entities allows a resonant interaction between them, a red emitting dye is obtained. In both cases, an intra-EET process takes place from fluorene to BODIPY core, which allows obtaining bright Vis emission under UV or Vis excitation. Thus, these dyes are versatile and efficient as active media in dye lasers, and could be applied in biology since the excitation and emission region are far away avoiding background interferences in the fluorescence signal detection. On the other hand, the attachment of indene to the BODIPY core, instead of fluorene, induces a drastic decrease in the fluorescence ability, but opens the way to development of a fluorescent sensor to detect iron cations.

Experimental Section

General: Starting materials and reagents used in the preparation of BODIPY dyes **1a–d** are commercially available unless their synthesis is described. The solvents were dried and distilled, before use. Spectral data of the known compounds were in accordance with the literature data. Flash column chromatography was performed by using silica gel Merck 60 (230–400 mesh). ^{1}H and ^{13}C NMR spectroscopy was recorded by using a Bruker Avance AV-500 spectrometer (500 MHz for ^{1}H and 125 MHz for ^{13}C), a Bruker Avance-DPX-300 spectrometer (300 MHz for ^{1}H and 75 MHz for ^{13}C) and a Bruker-AC-200 spectrometer (200 MHz for ^{1}H and 50 MHz for ^{13}C). All spectra were recorded in CDCl$_3$. ^{1}H chemical shifts are reported in ppm relative to tetramethylsilane ($\delta = 0.00$ ppm), using the residual solvent signal as the internal reference. The ^{13}C chemical shifts are reported in ppm with CDCl$_3$ ($\delta = 77.67$ ppm) as the internal standard. Chemical shift multiplicities are reported as s = singlet, d = doublet, t = triplet, q = quartet and m = multiplet. IR spectra (in cm^{-1}) were recorded by using a Bruker Tensor-27-FTIR spectrophotometer. Melting points were determined in open capillaries and are uncorrected. Mass spectra were registered by electron impact at 70 eV by using a VGI2–250 spectrometer. High resolution mass spectra were determined by electrospray ionisation in the positive mode (ESI$^+$) by using a Accurate-Mass Q-TOF LC/MS 6520 (Agilent Technologies). Combustion analyses (C, H, N) were obtained by using a LECO CHNS-932 apparatus at the Universidad Complutense de Madrid analysis services and were within 0.4% of the theoretical values.

General procedure for the synthesis of asymmetric BODIPYs 1a–d: To a solution of 2-acetyl-4-ethyl-3,5-dimethylpyrrole[8] (**2**) (1 equiv) in CHCl$_3$ was added POCl$_3$ (1.1 equiv), and the mixture was stirred for 30 min at RT. Then the corresponding pyrrole **3** (1 equiv) in CHCl$_3$ was added and the resulting solution was stirred for 12 h at RT. Triethylamine (1 equiv) was added, followed by an addition of BF$_3$·Et$_2$O (1 equiv), and stirring was continued for 3–4 h before being quenched with 10% aqueous HCl and extracted with CH$_2$Cl$_2$. The organic extracts were washed with water, dried over MgSO$_4$, filtered and evaporated to dryness. The dyes were isolated and purified by flash chromatography on silica gel.

Synthesis of 2-ethyl-4,4-difluoro-1,3,8-trimethyl-4-bora-3a,4a-diaza-*s*-indacene (1a): Compound **1a** was obtained through two synthetic routes: **Method A**: 2-Acetyl-4-ethyl-3,5-dimethylpyrrole (**2**) (455 mg, 2.8 mmol) in CHCl₃ (20 mL), POCl₃ (0.3 mL, 3.3 mmol), pyrrole (**3a**) (0.2 mL, 2.8 mmol) in CHCl₃ (10 mL), triethylamine (0.4 mL, 2.8 mmol) and BF₃·Et₂O (0.3 mL, 2.8 mmol) were reacted. Flash chromatography using hexane/EtAcO (98:2) afforded **1a** (190 mg, 26%) as a red solid and PM567 (35 mg, 4%).

Compound 1a: m.p. 155.5–156.0°C; ¹H NMR (300 MHz, CDCl₃): $\delta =$ 7.47 (br s, 1H, CH), 6.93 (d, $J = 3.6$ Hz, 1H, CH), 6.31 (dd, $J = 3.6$, 2.1 Hz, 1H, CH), 2.48 (s, 3H, CH₃), 2.46 (s, 3H, CH₃), 2.33 (q, $J = 7.5$ Hz, 2H, CH₂), 2.24 (s, 3H, CH₃), 0.97 ppm (t, $J = 7.5$ Hz, 3H, CH₃); ¹³C NMR (75 MHz, CDCl₃): $\delta = 160.3$ (C=N), 140.8 (C), 140.4 (2 C), 136.6 (CH), 135.1 (C), 134.1 (C), 122.7 (CH), 114.9 (CH), 17.0 (CH₂), 16.5 (CH₃), 14.5 (CH₃), 14.0 (CH₃), 13.1 ppm (CH₃); IR (neat): $\tilde{v} = 1568$ (C=N), 1455 cm⁻¹ (C=C); MS: *m/z* (%): 262 (38) [*M*]⁺, 247 (100), 227 (16); HR-MS-ESI⁺: calcd for (C₁₄H₁₇BF₂N₂+H⁺): 263.1532; found: 263.1428.

Method B: 2-Acetylpyrrole (1 g, 9.2 mmol) in CHCl₃ (20 mL), POCl₃ (1 mL, 10.1 mmol), 3-ethyl-2,4-dimethylpyrrole (1.13 g, 9.2 mmol) in CHCl₃ (20 mL), triethylamine (1.3 mL, 9.2 mmol) and BF₃·Et₂O (1.1 mL, 9.2 mmol) were allowed to react. Flash chromatography using hexane/EtAcO (98:2) afforded **1a** (1.1 g, 46%) and traces of BODIPY **6**.[11]

Synthesis of 2-[(*E*)-1*H*-inden-1-ylidenemethyl]-1*H*-pyrrole (3b): To a solution of indene (539 mg, 4.6 mmol) in dry THF (20 mL) at 0°C and under an argon atmosphere, was added dropwise a solution of *n*BuLi (3.2 mL, 1.6 M in hexane). The reaction mixture was stirred at RT for 1 h and then, a solution of **11** (1 g, 5.1 mmol) in dry THF (20 mL) was added. The mixture was refluxed for 4 h to complete the reaction and allowed to warm at RT before being quenched with saturated NH₄Cl solution and extracted with Et₂O. The combined organic phases were washed with H₂O, saturated NaHCO₃ solution and brine. The extract was dried over MgSO₄, filtered and concentrated to dryness. Flash chromatography using hexane/EtAcO (98:2) afforded **3b** (145 mg, 16%) as a yellow solid: m.p. 128.7–129.0°C; ¹H NMR (300 MHz, CDCl₃): $\delta = 8.44$ (br s, 1H, NH), 7.56–7.53 (m, 1H, CH), 7.27–7.24 (m, 1H, CH), 7.17–7.09 (m, 3H, 3 CH), 6.92–6.89 (m, 3H, 3 CH), 6.60 (br s, 1H, CH), 6.28–6.27 ppm (m, 1H, CH); ¹³C NMR (50 MHz, CDCl₃): $\delta = 141.4$ (C), 137.9 (C), 133.8 (C), 132.8 (C), 130.3 (C), 126.6 (CH), 125.2 (CH), 124.9 (CH), 122.4 (CH), 121.2 (CH), 118.7 (CH), 118.3 (CH), 114.9 (CH), 111.4 ppm (CH); IR (neat): $\tilde{v} = 3457$ (NH), 1640 cm⁻¹ (C=C); MS: *m/z* (%): 193 (87) [*M*]⁺, 192 (100), 165 (19), 95 (11); elemental analysis calcd (%) for C₁₄H₁₁N: C 87.01, H 5.74, N 7.25; found: C 87.03, H 5.71, N 7.26.

Synthesis of 2-ethyl-4,4-difluoro-5-indenylidene-1,3,8-trimethyl-4-bora-3a,4a-diaza-*s*-indacene (1b): 2-Acetyl-4-ethyl-3,5-dimethylpyrrole (**2**) (115 mg, 0.7 mmol) in CHCl₃ (10 mL), POCl₃ (0.07 mL, 0.8 mmol), pyrrole **3b** (140 mg, 0.7 mmol) in CHCl₃ (10 mL), triethylamine (0.1 mL, 0.7 mmol) and BF₃·Et₂O (0.09 mL, 0.7 mmol) were allowed to react. Flash chromatography using hexane/EtAcO (98:2) afforded **1b** (114 mg, 42%) as a blue solid: m.p. 286–287°C; ¹H NMR (300 MHz, CDCl₃): $\delta =$ 7.80 (br s, 1H, CH), 7.71–7.68 (m, 1H, CH), 7.21–7.11 (m, 3H, 3 CH), 7.02–6.85 (m, 4H, 4 CH), 2.55 (s, 3H, CH₃), 2.49 (s, 3H, CH₃), 2.36 (q, $J = 7.5$ Hz, 2H, CH₂), 2.28 (s, 3H, CH₃), 1.01 ppm (t, $J = 7.5$ Hz, 3H, CH₃); ¹³C NMR (75 MHz, CDCl₃): $\delta = 160.4$ (C=N), 147.3 (C), 141.9 (CH), 141.6 (2 C), 138.0 (C), 137.8 (CH), 136.2 (C), 135.0 (CH), 127.6 (CH), 125.9 (CH), 125.4 (CH), 123.6 (2 C), 121.1 (CH), 120.1 (CH), 119.0 (2 C), 118.4 (CH), 17.1 (CH₂), 16.4 (CH₃), 14.5 (CH₃), 14.0 (CH₃), 13.2 ppm (CH₃); IR (neat): $\tilde{v} = 1565$ (C=N), 1440 cm⁻¹; MS: *m/z* (%): 388 (100) [*M*]⁺, 373 (59); HR-MS-ESI⁺: calcd for (C₂₄H₂₃BF₂N₂+H⁺): 389.2001; found: 389.1997.

Synthesis of 2-[1*H*-fluoren-1-ylidenemethyl]-1*H*-pyrrole (3c): Compound **3c** was obtained through two synthetic routes. **Method A**: To a solution of fluorene (1.11 g, 6.7 mmol) in dry THF (40 mL) at 0°C and under an argon atmosphere, was added dropwise a solution of *n*BuLi (1.6 M in hexane) (4.8 mL, 7.6 mmol). The reaction mixture was stirred at RT for 1 h and then, a solution of **11** (1.44 g, 7.4 mmol) in dry THF (20 mL) was added. The mixture was refluxed for 4 h to complete the reaction and allowed to warm at RT before being quenched with saturated NH₄Cl solu-

tion and extracted with Et₂O. The combined organic phases were washed with H₂O, saturated NaHCO₃ solution and brine. The extract was dried over MgSO₄, filtered and concentrated to dryness. Flash chromatography using hexane/EtAcO (98:2) afforded **3c** (212 mg, 13%) as a beige solid and **3d** (329 mg, 12%) as a slightly yellow solid.

Compound 3c: m.p. 137.6–137.9°C; ¹H NMR (200 MHz, CDCl₃): $\delta = 8.57$ (br s, 1H, NH), 8.12 (d, $J = 7.6$ Hz, 1H, CH), 7.72–7.65 (m, 3H, 3 CH), 7.37 (br s, 1H, CH), 7.33–7.19 (m, 4H, 4 CH), 6.92 (br s, 1H, CH), 6.66 (br s, 1H, CH), 6.34–6.32 ppm (m, 1H, CH); ¹³C NMR (125 MHz, CDCl₃): $\delta = 141.2$ (C), 140.5 (C), 138.8 (C), 136.8 (C), 132.4 (C), 128.8 (C), 128.5 (CH), 127.8 (CH), 127.3 (CH), 123.5 (CH), 120.8 (CH), 120.7 (CH), 120.4 (CH), 120.1 (CH), 120.0 (CH), 117.3 (CH), 114.3 (CH), 111.1 ppm (CH); IR (neat): $\tilde{v} = 3460$ (NH), 1580 cm⁻¹ (C=C); MS: *m/z* (%): 243 (82) [*M*]⁺, 242 (100), 215 (10); elemental analysis calcd (%) for C₁₈H₁₃N: C 88.86, H 5.39, N 5.76; found: C 88.84, H 5.38, N 5.78.

Compound 3d: m.p. 165.0–166.0°C; ¹H NMR (300 MHz, CDCl₃): $\delta =$ 7.70–7.65 (m, 4H, NH, 3 CH), 7.54–7.52 (m, 2H, 2 CH), 7.34–7.09 (m, 9H, 9 CH), 6.93–6.90 (m, 2H, 2 CH), 6.16–6.14 (m, 1H, CH), 5.70–5.67 (m, 1H, CH), 5.26–5.20 (m, 1H, CH), 4.73 (d, $J = 7.5$ Hz, 2H, 2 CH), 3.29 ppm (t, $J = 7.5$ Hz, 1H, CH); ¹³C NMR (75 MHz, CDCl₃): $\delta = 144.6$ (2 C), 144.2 (C), 144.0 (C), 141.7 (2 C), 141.2 (2 C), 128.3 (2 CH), 128.0 (2 CH), 127.2 (4 CH), 125.3 (4 CH), 123.3 (C), 120.5 (2 CH), 120.4 (2 CH), 120.3 (CH), 114.1 (CH), 94.9 (CH), 50.0 (2 CH), 48.2 ppm (CH); IR (neat): $\tilde{v} = 3457$ (NH), 1570 cm⁻¹ (C=C); MS: *m/z* (%): 409 (1) [*M*]⁺, 244 (100), 165 (19); elemental analysis calcd (%) for C₃₁H₂₃N: C 90.92, H 5.66, N 3.42; found: C 90.95, H 5.64, N 3.41.

Method B: To a stirred suspension of (bromomethyl)triphenylphosphonium bromide (4.46 g, 10.2 mmol) in THF (60 mL) under argon and at −60°C was added sodium bis(hexamethylsilyl)amide (6 mL, 2.0 M in THF). The resulting red solution was stirred at −60°C for 40 min, and then a solution of fluorenone (1.66 g, 9.2 mmol) in THF (10 mL) was added. It was allowed to warm slowly to RT and stirred overnight before being quenched with H₂O and extracted with Et₂O. The extract was dried over MgSO₄, filtered and concentrated to dryness. Flash chromatography using hexane afforded **16**[12] (2.27 g, 96%) as a yellow solid. ¹H NMR (200 MHz, CDCl₃): $\delta = 8.58$ (d, $J = 7.8$ Hz, 1H, CH), 7.72 (d, $J = 7.8$ Hz, 1H, CH), 7.68 (d, $J = 7.8$ Hz, 1H, CH), 7.57 (d, $J = 7.8$ Hz, 1H, CH), 7.45 (dt, $J = 7.7$, 1.4 Hz, 1H, CH), 7.40 (s, 1H, CH), 7.39–7.34 (m, 2H), 7.28 ppm (dt, $J = 7.8$, 0.8 Hz, 1H, CH).

To a solution of **16** (601 mg, 2.3 mmol) in DME (30 mL) under an argon atmosphere, were added **15** (494 mg, 2.3 mmol) and Na₂CO₃ (297 mg, 2.8 mmol) in the presence of a catalytic amount of tetrakis(triphenylphosphine)palladium (8.6 mg, 0.008 mmol). The reaction mixture was refluxed for 38 h to complete the reaction and allowed to warm at RT before being quenched with H₂O and extracted with CH₂Cl₂. The extract was dried over MgSO₄, filtered and concentrated to dryness. Flash chromatography using hexane/Et₂O (99:1) afforded **3c** (74 mg, 13%).

Synthesis of 2-ethyl-4,4-difluoro-5-fluorenylidene-1,3,8-trimethyl-4-bora-3a,4a-diaza-*s*-indacene (1c): 2-Acetyl-4-ethyl-3,5-dimethylpyrrole (**2**) (65 mg, 0.4 mmol) in CHCl₃ (10 mL), POCl₃ (0.04 mL, 1.1 mmol), pyrrole **3c** (97 mg, 0.4 mmol) in CHCl₃ (10 mL), triethylamine (0.06 mL, 0.4 mmol) and BF₃·Et₂O (0.05 mL, 0.4 mmol) were allowed to react. Flash chromatography using hexane/EtAcO (98:2) afforded **1c** (26 mg, 15%) as a blue solid: m.p. 277–278°C; ¹H NMR (200 MHz, CDCl₃): $\delta =$ 8.20 (d, $J = 7.7$ Hz, 1H, CH), 7.87 (br s, 1H, CH), 7.81–7.78 (m, 1H, CH), 7.65–7.58 (m, 2H, 2 CH), 7.26–7.03 (m, 6H, 6 CH), 2.53 (s, 3H, CH₃), 2.52 (s, 3H, CH₃), 2.35 (q, $J = 7.5$ Hz, 2H, CH₂), 2.28 (s, 3H, CH₃), 1.00 ppm (t, $J = 7.5$ Hz, 3H, CH₃); ¹³C NMR (50 MHz, CDCl₃): $\delta = 160.3$ (C=N), 146.4 (C), 141.5 (C), 140.3 (C), 140.0 (C), 138.8 (C), 138.2 (C), 138.0 (C), 136.3 (C), 136.0 (C), 135.5 (CH), 134.6 (C), 128.8 (CH), 128.4 (CH), 127.1 (CH), 126.7 (CH), 125.0 (CH), 122.7 (CH), 121.0 (CH), 119.8 (CH), 119.5 (CH), 119.1 (CH), 117.4 (CH), 17.0 (CH₂), 16.3 (CH₃), 14.5 (CH₃), 13.9 (CH₃), 13.1 ppm (CH₃); IR (neat): $\tilde{v} = 1568$ (C=N), 1447 cm⁻¹ (C=C); MS: *m/z* (%): 438 (3) [*M*]⁺, 322 (13), 85 (51), 71(67), 57 (100); HR-MS-ESI⁺: calcd for (C₂₈H₂₅BF₂N₂+H⁺): 439.2158; found: 439.2154.

Synthesis of 2-ethyl-4,4-difluoro-5-(di-9*H*-fluoren-9-ylmetyl)-1,3,8-trimethyl-4-bora-3a,4a-diaza-*s*-indacene (1d): 2-Acetyl-4-ethyl-3,5-dimethyl-

pyrrole (**2**) (66 mg, 0.4 mmol) in CHCl$_3$ (10 mL), POCl$_3$ (0.04 mL, 1.1 mmol), pyrrole **3d** (164 mg, 0.4 mmol) in CHCl$_3$ (10 mL), triethylamine (0.06 mL, 0.4 mmol) and BF$_3$·Et$_2$O (0.05 mL, 0.4 mmol) were reacted. Flash chromatography using hexane/EtAcO (98:2) afforded **1d** (100 mg, 40%) as an orange solid: m.p. 318–319°C; ^{1}H NMR (300 MHz, CDCl$_3$): $\delta = 7.63$–7.60 (m, 4H, 4 CH), 7.36 (d, $J = 7.5$ Hz, 2H, 2 CH), 7.28–7.04 (m, 6H, 7 CH), 7.02–6.99 (m, 2H, 2 CH), 6.76 (d, $J = 7.5$ Hz, 2H, 2 CH), 6.59 (d, $J = 4.2$ Hz, 1H, CH), 5.40 (t, $J = 4.2$ Hz, 1H, CH), 5.14 (d, $J = 4.2$ Hz, 1H, CH), 4.42 (d, $J = 4.2$ Hz, 2H, 2 CH), 2.53 (s, 3H, CH$_3$), 2.32 (s, 3H, CH$_3$), 2.30 (q, $J = 7.5$ Hz, 2H, CH$_2$), 2.18 (s, 3H, CH$_3$), 0.95 ppm (t, $J = 7.5$ Hz, 3H, CH$_3$); ^{13}C NMR (75 MHz, CDCl$_3$): $\delta = 157.8$ (C=N), 154.5 (C), 145.8 (2 C), 145.3 (4 C), 141.8 (4 C), 141.4 (2 C), 139.1 (C), 127.1 (2 CH), 126.9 (2 CH), 126.6 (2 CH), 126.5 (2 CH), 126.4 (2 CH), 125.9 (2 CH), 119.6 (2 CH), 119.5 (2 CH), 116.5 (CH), 49.7 (2 CH), 44.8 (CH), 17.0 (CH$_2$), 16.4 (CH$_3$), 14.6 (CH$_3$), 13.8 (CH$_3$), 13.0 ppm (CH$_3$); IR (neat): $\tilde{\nu} = 1572$ (C=N), 1447 cm^{-1} (C=C); MS: m/z (%): 439 (52) $[M]^+$−165, 419 (100), 165 (35), 57 (29); HR-MS-ESI$^+$: calcd for (C$_{41}$H$_{35}$BF$_2$N$_2$+H$^+$): 605.2940; found: 605.2936.

X-ray structures: The structures of the dyes **1b–d** were determined by using single crystal X-ray diffraction. The quality of the data for the dyes **1b** and **1c** are poor, but there were not possible to obtain crystals of better quality. The data collections were realised at low temperature and using Cu radiation to improve the quality of the data.

CCDC 783761 (**1a**), 783762 (**1b**) and 783763 (**1c**) contain the supplementary crystallographic data for this paper. These data can be obtained free of charge from The Cambridge Crystallographic Data Centre via www.ccdc.cam.ac.uk/data_request/cif.

Photophysical properties: The photophysical properties were registered in diluted solutions (around 2×10^{-6} M), prepared by adding the corresponding solvent to the residue from the adequate amount of a concentrated stock solution in acetone, after vacuum evaporation of this solvent. UV/Vis absorption and fluorescence spectra were recorded by using a Cary 4E spectrophotometer and a SPEX Fluorolog 3–22 spectrofluorimeter, respectively. Fluorescence quantum yields (ϕ) were evaluated from corrected spectra by using a diluted methanol solution of the commercial PM567 ($\phi = 0.91$)[32] and PM650 ($\phi = 0.06$)[33] as reference, depending of the absorption and emission region of the considered BDP. Radiative decay curves were registered by using the time correlated single-photon counting technique (Edinburgh Instruments, model FL920). Fluorescence emission was monitored at the maximum emission wavelength after excitation at $\lambda = 470$ nm by means of a diode laser (PicoQuant, model LDH470) with 150 ps FWHM pulses. The fluorescence lifetime (τ) was obtained after the deconvolution of the instrumental response signal from the recorded decay curves by means of an iterative method. The goodness of the exponential fit was controlled by statistical parameters (chi-square, Durbin–Watson and the analysis of the residuals). The rate constant of radiative (k_{fl}) and non-radiative (k_{nr}) deactivations were calculated by means of Equation (1).

$$k_{fl} = \phi/\tau \text{ and } k_{nr} = (1-\phi)/\tau \tag{1}$$

The ground state geometry was optimised by using the B3LYP method and the double valence basis set (6-31G) implemented in the Gaussian 03 software. The energy minimisation process was performed without any geometrical restrictions, and it was considered to be adequately concluded when the analysis of the vibrational frequencies did not give any negative frequency. The absorption properties were simulated by the time-dependent (TD) method together with the above-cited density functional theory (B3LYP).

Laser experiments: The commercial laser dyes Coumarin 503 (also called Coumarin 307), Coumarin 522, Coumarin 540 A (also called Coumarin 153) and Pirromethene 597 (laser grade, Exciton) were used as received with a purity of >99% (checked by spectroscopic and chromatographic methods). Solvents for laser studies were of spectroscopic grade (Merck, Aldrich or Sigma) and were used without purification. The new dyes were incorporated in homopolymers, such as PMMA and PHEMA as well as in linear copolymers obtained by copolymerisation of MMA with different volumetric proportions HEMA. All monomers were purchased from Aldrich. MMA and the initiator: 2,2'-azobisisobutyronitrile (AIBN) (Acros) were purified before use while HEMA was used as received.

Preparation of solid polymeric samples: The new BDP derivatives were incorporated into the different solid matrices following the procedure previously described.[34] The solid monolith laser samples were cast in cylindrical shape, forming rods of 10 mm diameter and 10 mm length. A cut was made parallel to the axis of cylinder to obtain a lateral flat surface of approximately 6×10 mm. This surface, as well as the ends of the laser rods, was prepared for lasing experiments by using a grinding and polishing machine (Phoenix Beta 4000, Büehler) until optical-grade finished. The planar grinding stage was carried out by using a Texmet 1000 sand paper (Buehler) with a diamond polishing compound of 6 µm as an abrasive in mineral oil as a lubricant. The final polishing stage was realised with a G-Tuch Microcloth (Buehler), using a cloth disk Mastertex (Buehler) with diamond of 1 µm in mineral oil as an abrasive type.

Liquid solutions of dyes were contained in 1 cm optical-path quartz cells that were carefully sealed to avoid solvent evaporation during experiments. The solutions of the newly synthesised dyes as well as the solid samples doped with these new dyes were transversely pumped at different wavelengths matching the maximum absorption of the corresponding dyes: at $\lambda = 532$ nm, with 5 mJ per pulse, 6 ns FWHM pulses from a frequency-doubled Q-switched Nd:YAG laser (Monocrom OPL-10) and at $\lambda = 500$, 515 and 577 nm, with 5 mJ, 12 ns FWHM pulses from a Nd-YAG-pumped dye laser (Spectron SL800 with an ethanolic solution of Coumarin 503, Coumarin 522 and Pyrromethene 597, respectively). The exciting pulses were line-focused onto the cell, providing pump fluences on the active medium of 180 mJ cm^{-2}. The oscillation cavity (2 cm length) consisted of a 90% reflectivity aluminium mirror, with the lateral face of the cell as output coupler.

The photostability of each dye in liquid phase was also evaluated under experimental conditions identical to those selected to irradiate the fluorophores embedded in solid polymeric matrices, which will allow later comparison of their stability in liquid and solid phases under laser irradiation. Because the irradiated volume in solid samples was estimated to be 10 µL, capillary tubes into which ethyl acetate solutions of dyes were incorporated offer the best geometry to reproduce the volume irradiated in the solid samples, thus maintaining the same laser pump conditions in both cases. Although the low optical quality of the capillary prevents laser emission from the dyes, information about photostabilities can be obtained by monitoring the decrease in laser-induced fluorescence intensity, excited transversally to the capillary, as a function of the number of pump pulses at 10 Hz repetition rate. The fluorescence emission was monitored perpendicular to the exciting beam, and its collection and analysis was carried out with the same set-up selected to characterise the laser emission from dyes incorporated into solid samples.

Acknowledgements

[1] a) A. Costela, I. Garcia-Moreno, R. Sastre in *Handbook of Advanced Electronic and Photonic Materials and Devices, Vol. 7* (Ed.: H. S. Nalwa), Academic, San Diego, 2001, Chapter 4, p. 161; b) A. Costela, I. García-Moreno, R. Sastre, *Phys. Chem. Chem. Phys* 2003, *5*, 4745–4763; c) J. Bañuelos Prieto, F. López Arbeloa, V. Martínez Martínez, T. López Arbeloa, I. López Arbeloa, *J. Phys. Chem. A* 2004, *108*, 5503–5508; d) F. López Arbeloa, J. Bañuelos, V. Martínez, T. Arbeloa, I. López Arbeloa, *Int. Rev. Phys. Chem.* 2005, *24*,

FULL PAPER

339–374; e) A. Costela, I. García-Moreno, C. Gómez, O. García, R. Sastre, A. Roig, E. Molins, *J. Phys. Chem. B* **2005**, *109*, 4475–4480; f) O. García, R. Sastre, D. del Agua, A. Costela, I. García-Moreno, *Chem. Mater.* **2006**, *18*, 601–602; g) M. Álvarez, A. Costela, I. García-Moreno, F. Amat-Guerri, M. Liras, R. Sastre, F. López Arbeloa, J. Bañuelos Prieto, I. López Arbeloa, *Photochem. Photobiol. Sci.* **2008**, *7*, 802–813.

[2] S. C. Guggenheimer, J. H. Boyer, K. Thangaraj, M. Shah, M.-L. Soong, T. G. Pavlopoulos, *Appl. Opt.* **1993**, *32*, 3942–3943.

[3] a) T. G. Pavlopoulos, J. H. Boyer, M. Shah, K. Thangaraj, M.-L. Soong, *Appl. Opt.* **1990**, *29*, 3885–3889; b) G. H. Jones, S. Kumar, O. Klueva, D. Pacheco, *J. Phys. Chem. A* **2003**, *107*, 8429–8434; c) A. Loudet, K. Burgess, *Chem. Rev.* **2007**, *107*, 4891–4932; d) S. Mula, A. K. Ray, M. Banerjee, T. Chaudhuri, K. Dasgupta, S. Chattopadhyay, *J. Org. Chem.* **2008**, *73*, 2146–2154; e) A. Costela, I. García-Moreno, M. Pintado-Sierra, F. Amat-Guerri, M. Liras, R. Sastre, F. López Arbeloa, J. Bañuelos Prieto, I. López Arbeloa, *J. Photochem. Photobiol. A* **2008**, *198*, 192–199; f) G. Ulrich, R. Ziessel, A. Harriman, *Angew. Chem.* **2008**, *120*, 1202–1219; *Angew. Chem. Int. Ed.* **2008**, *47*, 1184–1201.

[4] T. Kowada, S. Yamaguchi, K. Ohe, *Org. Lett.* **2010**, *12*, 296–298.

[5] a) A. Nagai, J. Miyake, K. Kokado, Y. Nagata, Y. Chujo, *J. Am. Chem. Soc.* **2008**, *130*, 15276–15278; b) G. Meng, S. Velayudham, A. Smith, R. Luck, H. Liu, *Macromolecules* **2009**, *42*, 1995–2001; c) V. R. Donuru, G. K. Vegesna, S. Velayudham, S. Green, H. Liu, *Chem. Mater.* **2009**, *21*, 2130–2138.

[6] a) C. Goze, G. Ulrich, R. Ziessel, *J. Org. Chem.* **2007**, *72*, 313–322; b) S. Goeb, R. Ziessel, *Tetrahedron Lett.* **2008**, *49*, 2569–2574; c) A. Harriman, L. J. Mallon, S. Goeb, G. Ulrich, R. Ziessel, *Chem. Eur. J.* **2009**, *15*, 4553–4564; d) T. Bura, R. Ziessel, *Tetrahedron Lett.* **2010**, *51*, 2875–2879.

[7] D. Armesto, M. G. Gallego, W. M. Horspool, A. R. Agarrabeitia, *Tetrahedron* **1995**, *51*, 9223–9240.

[8] G. G. Kleinspehn, A. H. Corwin, *J. Org. Chem.* **1960**, *25*, 1048–1050.

[9] N. Ono, T. Yamamoto, N. Shimada, K. Kuroki, M. Wada, R. Utsunomiya, T. Yano, H. Uno, T. Murashima, *Heterocycles* **2003**, *61*, 433–447.

[10] J. Clayden, N. Greeves, S. Warren, P. Wothers in *Organic Chemistry*, Oxford University Press, Oxford, **2001**, p. 1159.

[11] D.-C. Wang, H.-P. Wang, S. Gao, T.-Y. Zhang, X.-J. Peng, *Acta Crystallogr. Sect. E* **2007**, *63*, o2238–o2239.

[12] G. C. Paul, J. J. Gajewski, *Synthesis* **1997**, 524–526.

[13] a) A. Burghart, H. Kim, M. B. Welch, L. H. Thoresen, J. R. Reibenspies, K. Burgess, F. Bergström, L. B.-A. Johansson, *J. Org. Chem.* **1999**, *64*, 7813–7819; b) J. Chen, A. Burghart, A. Derecskei-Kovacs, K. Burgess, *J. Org. Chem.* **2000**, *65*, 2900–2906.

[14] a) Q. Zheng, G. Xu, P. N. Prasad, *Chem. Eur. J.* **2008**, *14*, 5812–5819; b) S. Mula, A. K. Ray, M. Banerjee, T. Chaudhuri, K. Dasgupta, S. Chattopadhyay, *J. Org. Chem.* **2008**, *73*, 2146–2154; c) T. T. Vu, S. Badré, C. Dumas-Verdes, J.-J. Vachon, C. Julien, P. Audebert, E. Y. Senotrusova, E. Y. Schmidt, B. A. Trofimov, R. B. Pansu, G. Clavier, R. Méallet-Renault, *J. Phys. Chem. C* **2009**, *113*, 11844–11855.

[15] S. A. Pérez Guarín, S. Dufresne, D. Tsang, A. Sylla, W. G. Skene, *J. Mater. Chem.* **2007**, *17*, 2801–2811.

[16] a) R. K. Lammi, A. Ambroise, T. Balasubramanian, R. W. Wagner, D. F. Bocian, D. Holten, J. S. Lindsey, *J. Am. Chem. Soc.* **2000**, *122*, 7579–7591; b) R. K. Lammi, R. W. Wagner, A. Ambroise, J. R. Diers, D. F. Bocian, D. Holten, J. S. Lindsey, *J. Phys. Chem. B* **2001**, *105*, 5341–5352; c) C.-W. Wan, A. Burghart, J. Chen, F. Bergström, L. B.-A. Johansson, M. F. Wolford, T. G. Kim, M. R. Topp, R. M. Hochtrasser, K. Burgess, *Chem. Eur. J.* **2003**, *9*, 4430–4441; d) D. Kumaresan, A. Datta, M. Ravikanth, *Chem. Phys. Lett.* **2004**, *395*, 87–91; e) R. Ziessel, C. Goze, G. Ulrich, M. Césario, P. Retailleau, A. Harriman, J. P. Rostron, *Chem. Eur. J.* **2005**, *11*, 7366–7378.

[17] S. Speiser, *Chem. Rev.* **1996**, *96*, 1953–1976.

[18] a) G. D. Scholes, K. P. Ghiggino, A. M. Oliver, M. N. Paddon-Row, *J. Am. Chem. Soc.* **1993**, *115*, 4345–4349; b) K. P. Ghiggino, E. K. L. Yeow, D. J. Haines, G. D. Scholes, T. A. Smith, *J. Photochem. Photobiol. A* **1996**, *102*, 81–86.

[19] J. Bañuelos, F. López Arbeloa, T. Arbeloa, S. Salleres, F. Amat-Guerri, M. Liras, I. López Arbeloa, *J. Phys. Chem. A* **2008**, *112*, 10816–10822.

[20] J. R. Lakowiczr in *Principles of Fluorescence Spectroscopy*, 3rd ed., Springer, New York, **2006**.

[21] a) C. Reichardt, *Chem. Rev.* **1994**, *94*, 2319–2358; b) A. R. Katritzky, D. C. Fara, H. Yang, K. Tämm, *Chem. Rev.* **2004**, *104*, 175–198.

[22] a) M. J. Kamlet, R. W. Taft, *J. Am. Chem. Soc.* **1976**, *98*, 377–383; b) M. J. Kamlet, R. W. Taft, *J. Am. Chem. Soc.* **1976**, *98*, 2886–2894; c) M. J. Kamlet, J. L. M. Abboud, R. W. Taft, *J. Am. Chem. Soc.* **1977**, *99*, 6027–6038.

[23] J. Catalan, *J. Phys. Chem. B* **2009**, *113*, 5951–5960.

[24] T. G. Pavlopoulos, *Prog. Quantum Electron.* **2002**, *26*, 193–224.

[25] T. Waugh, H. Morrison, *J. Am. Chem. Soc.* **1999**, *121*, 3083–3092.

[26] M. J. Bearpark, F. Bernardi, M. Olivucci, M. A. Robb, *J. Phys. Chem. A* **1997**, *101*, 8395–8401.

[27] a) A. Togni, T. Hayashi, *Ferrocene*, Wiley-VCH, Weinheim, **1995**; b) B. R. Waldbaum, R. C. Kerber, *Inorg. Chim. Acta* **1999**, *291*, 109–126.

[28] a) K. Rurack, M. Kollmannsberger, U. Resch-Genger, *J. Am. Chem. Soc.* **2000**, *122*, 968–969; b) R. Méallet-Renault, R. Pansu, S. Amigoni-Gerbier, C. Larpent, *Chem. Commun.* **2004**, 2344–2345; c) K. Yamada, Y. Nomura, D. Citterio, N. Iwasawa, K. Suzuki, *J. Am. Chem. Soc.* **2005**, *127*, 6956–6957; d) J. L. Bricks, A. Kovalchuk, C. Trieflinger, M. Nofz, M. Büschel, A. I. Tolmachev, J. Daub, K. Rurack, *J. Am. Chem. Soc.* **2005**, *127*, 13522–13529; e) T. Kálai, K. Hideg, *Tetrahedron* **2006**, *62*, 10352–10360.

[29] F. Wilkinson, D. J. Mcgarvey, A. F. Olea, *J. Phys. Chem.* **1994**, *98*, 3762–3769.

[30] A. Costela, I. García-Moreno, J. M. Figuera, F. Amat-Guerri, R. Mallavia, M. D. Santa María, R. Sastre, *J. Appl. Phys.* **1996**, *80*, 3167–3173.

[31] N. N. Barashkov, O. A. Gonder, *Fluorescence Polymers*, Ellis Horwood, Chichester, **1994**.

[32] F. López Arbeloa, T. López Arbeloa, I. López Arbeloa, I. García-Moreno, A. Costela, R. Sastre, F. Amat-Guerri, *Chem. Phys.* **1998**, *236*, 331–341.

[33] F. López Arbeloa, J. Bañuelos, V. Martínez, T. Arbeloa, I. López Arbeloa, *ChemPhysChem* **2004**, *5*, 1762–1771.

[34] M. Álvarez, F. Amat-Guerri, A. Costela, I. García-Moreno, C. Gómez, M. Liras, R. Sastre, *Appl. Phys. B* **2005**, *80*, 993–1006.